Check for updates

Insight into carbon quantum dot–vesicles interactions: role of functional groups†

Jayanta S. Boruah,[ab] Kamatchi Sankaranarayanan[c] and Devasish Chowdhury [iD] *[a]

Understanding carbon quantum dot–cell membrane interaction is essential for designing an effective nanoparticle-based drug delivery system. In this study, an attempt has been made to study the interaction involving phosphatidylcholine vesicles (PHOS VES, as model cell membrane) and four different carbon quantum dots bearing different functional groups ($-COOH$, $-NH_2$, $-OH$, and protein bovine serum albumin coated) using various tools such as PL behavior, surface charge on vesicles, QCM, ITC, TEM, LSV, and FTIR. From the above studies, it was observed that the $-NH_2$ terminating carbon dots were capable of binding strongly with the vesicles whereas other functional groups bearing carbon dots were not significantly interacting. This observation was also supported by direct visual evidence as shown by transmission electron microscopy, which shows that the polyethyleneimine carbon dot (PEICD) bearing $-NH_2$ functionality has greater affinity towards PHOS VES. The mechanistic insight presented in the paper indicates greater possibility of higher H-bonding, signifying better interaction between $-NH_2$ functionalized carbon dots and PHOS VES supported by FTIR, QCM, ITC and TEM. Moreover, the transport of neurotransmitters (which are generally amine compound) in neurons for cellular communication through synapse is only possible through vesicular platforms, showing that in our body, such interactions are already present. Such studies on the nano–bio interface will help biomedical researchers design efficient carbon-based nanomaterial as drug/gene delivery vehicles.

Introduction

It is interesting to note that vesicles are one of the potential classes of bio-mimicking materials acting as standard cell models. The importance of vesicles stands at their dynamic structure and properties with multiple functions. They can be extracted naturally from bacteria or constructed synthetically from chemicals. The basic ingredients for their formation (synthetically) are mainly fatty acids, lipids, phospholipids, surfactant, polymers, and others.[1–3] A popular member of this family is the liposome, which can be synthesized from lipids and phospholipids, and is gradually becoming one of the most studied systems in biomedical research. As a natural process, bacteria can also produce vesicles as a metabolic product known as outer membrane vesicles (OMVs), which are actually responsible for their cellular communication. It can be extracted employing standard protocols.[4] Its spherical structure (both natural or synthetic) is composed of a bilayer of basic

components resembling the structure of our cell membrane. The maintenance of stability and properties of vesicles can be achieved by different factors, such as pH,[5] temperature,[6] light,[7] dispersing medium,[8] and functionalization.[9] The biocompatibility nature of such vesicles is the prime feature for their use in biomedical fields, including drug delivery,[10] vaccine,[11] and biosensing.[12] In fact, the pharmacokinetics and pharmacodynamics behavior of vesicles during drug delivery were studied earlier.[13] Nowadays, the functionalization of vesicles has been attempted to step up the functional efficacy of these systems. Vesicles were reported to have low loading capacity for any biomolecule or drug. Therefore, researchers have been searching for other entities to incorporate, such as hybrid vesicles. The application of protein, enzyme, DNA, and RNA attachment into vesicles for making superior materials has been explored worldwide.[14,15] However, another class of substances, "nanomaterials" (mainly, carbon-based) are such target molecules, designed to have the desired functional groups, which in turn render the vesicles with appropriate functionality and enhanced functional efficiency. Carbon dots (particle size below 10 nm) are one such member with interesting optical (fluorescence), chemical, magnetic, electrical and mechanical properties.[16,17] The selection of nanoparticles for this purpose of nanoconjugate preparation stems from the fact that they have high surface-to-volume ratio bearing a large surface area. The outstanding properties of such nanomaterials have been exploited by numerous researchers in

[a]Material Nanochemistry Laboratory, Physical Sciences Division, Institute of Advanced Study in Science and Technology, Paschim Boragaon, Garchuk, Guwahati, 781035, India

[b]Department of Chemistry, Cotton University, Guwahati, Assam, India

[c]Physical Sciences Division, Institute of Advanced Study in Science and Technology, Paschim Boragaon, Garchuk, Guwahati, 781035, India. E-mail: devasish@iasst.gov.in

† Electronic supplementary information (ESI) available. See DOI: 10.1039/d1ra08809b

biomedicine, gene therapies, bio-imaging, diagnostics and pharmacokinetics studies.[18-20] In order to accomplish these applications, it is required to undergo proper interaction of nanomaterials and cells, which of course, is dependent on the versatile properties of the nanomaterials.[21] To imbibe the justification and superiority of the nanoparticles into vesicles in terms of their application, researchers are working to make various nanocomposites. It is also relevant to prevent the nanoparticles to adsorb the protein, while entering the body fluid, changing the physiological operation. Protein corona formation by nanoparticles is associated with cytotoxicity.[22] There are many reports on the fabrication of nanocomposites from vesicles and nanoparticles exhibiting significant results.[23,24] The biomimicking characteristic of vesicles helps in circulating the nanoparticles in the body fluid without any disturbance, thereby enhancing the capacity of the drug or biomolecule loading.[25] It is important to note that although the study on nanoparticle–cell interaction has been done using cell lines employing various biological experiments,[21] it is necessary to examine the way that nanoparticles interact with cells, and the factors responsible for that. The size-dependent cellular uptake of a protein-coated graphene oxide nanosheet was studied on C2C12 cell lines.[26] Many such examples of the effect of nanoparticles on the cell surfaces (owing to factors like size, stability, precursor, type of bonding) have been put forward by an earlier report.[27] There are some theoretical reports describing the process of nanoparticle internalization by vesicles and relevant factors.[28,29] Previously, researchers demonstrated nanoparticle–cell interaction using vesicles and polymer-coated core–shell type magnetic nanoparticles, and proposed some unusual behavior occurring on the surface of the vesicles.[30] Recently, the impact of the aluminium oxide nanoparticle on the liposome was put forwarded, considering the scattering phenomenon.[31] A combined experimental and computational study published recently revealed that on incorporating hydrophobicity into the nanoparticles, the nano–bio interaction is dependent on the nanoparticles' size and membrane surface tension.[32] However, until now, no strong evidence of interaction of the carbon nanomaterials with the cell membrane (or vesicles) is there, except for one recent report where carbon dots (amine group terminating) from three different isomers of phenylenediamine (*ortho*, *meta* and *para*) interacted with the vesicles and only the *o*-isomer was found to be embedded on the vesicles.[33] In this context, particularly, the functional groups present on the carbon-based nanomaterials is expected to have some role in the cellular interaction. It is obvious that the inclusion of all type of nanoparticles may not lead to an upgraded output. It is worth noting that dissipative particle dynamics simulations study revealed the tension-induced rupture of the phospholipid membrane, which encapsulated the hydrophobic nanoparticles.[34] So, the nanoparticles may be destructive to the cellular membrane and hence, the design of the nanoparticles should be delicately chosen to fabricate the nanocomposites.

Through this work, an attempt has been made to address the following questions. (1) How do the carbon quantum dots (carbon nanomaterial) interact with the model cell membrane (vesicles)? (2) Does the functionality of the quantum dots have any role in the possible interaction? (3) What if the carbon quantum dot is not bare, but rather coated with a protein and has a possible interaction with the vesicles? (4) What factors does the interaction depend on? In this work, four different carbon dots (a type of carbon nanomaterial) having functionalities –COOH, –NH$_2$, –OH and protein-coated (amino acid) were interacted with phospholipid vesicles individually. In this work, phospholipid vesicles were taken as a model cell membrane as a result of its strong resemblance in chemical composition to that of the native cell membrane. The carbon dots were synthesized from citric acid, polyethyleneimine, polyethylene glycol and the last one with polyethylene glycol coated with protein (bovine serum albumin, BSA) to introduce the respective functionalities in the carbon dots. A UV-Visible spectrophotometer, the photoluminescence property of the carbon dots, zeta potential measurement, quartz crystal microbalance (QCM) and isothermal titration calorimetry (ITC) were utilized as investigating tools for the nano–bio interaction study. The results were finally supported by transmission electron microscopy (TEM), FTIR and linear sweep voltammetry (LSV) study. The possible mechanism is also discussed in the paper.

Experimental

Materials and methods

Phosphatidylcholine from egg yolk and polyethyleneimine ($M_w \sim 25\,000$) were procured from Sigma Aldrich, India. Chloroform, sodium hydroxide and ammonia solution (25%) were used from Merck, India. Citric acid, polyethylene glycol 6000 and bovine serum albumin (BSA) were purchased from SRL, India. Water used in all of the experiments was from the Merck Elix Millipore system. All of the chemicals were employed without further purification. Optics technology UV lamp (India) was used in determining the visual fluorescence characteristic of the materials.

Preparation of the phosphatidylcholine vesicles (PHOS VES)

A modified film hydration method reported by Murakami *et al.*[35] was used for the fabrication of the phosphatidylcholine vesicles. Typically, 3.6 mg of the phospholipid is dissolved in 2 mL chloroform in a round bottom flask. Then, the solvent is evaporated from the vessel under vacuum using a rotary evaporator (Buchi R210) at a temperature of 40 °C. Consequently, a homogenous film appeared on the surface of the flask, which was kept in a desiccator overnight to make the film dry or solvent-free. Subsequently, 10 mL Milli-Q water was added to the flask and a turbid dispersion was formed on shaking, resulting in the formation of vesicles. It was sonicated for 1 h at room temperature in a bath sonicator to give rise to a dispersion of small-sized vesicles in water. The concentration of the vesicles was 10^{-4} M and it was stored at 4 °C temperature until use.

Preparation of citric acid carbon dot (CACD, with –COOH functional group)

Fabrication of the citric acid carbon dots was performed with the help of a reported method.[36] Basically, 4.2 g of citric acid

(anhydrous) was taken in a 50 mL round-bottomed flask and heated in an oil bath at a temperature of 180 °C with mild stirring (100 rpm). The solid sample was melted completely within 2–3 min and kept on heating until 120 min. In the first 15 min of heating, the colorless liquid turned into a light yellow color, and gradually changed to an orange-yellow color by the completion of the reaction time. The resultant material (carbon dot, CACD) was dense and sticky (orange colored), and transferred to a Petri dish. It was solidified at room temperature and stored at 4 °C temperature until use. The solid carbon dot was dispersed in a particular volume of water and used further after neutralizing to pH 7. The CACD dispersion showed a light green fluorescence under UV light (365 nm).

Preparation of the polyethyleneimine carbon dot (PEICD, with –NH$_2$ functional group)

The preparation of the polyethyleneimine carbon dot (PEICD) involved a modification of the reaction condition proposed by Han *et al.* to synthesize the same material.[37] Simply, a 100 mg mL^{-1} of PEI ($M_w \sim 25\,000$) solution was made in 8 mL ultrapure water through stirring for 10 min at room temperature. Unlike the earlier report (where people used a Teflon-lined stainless-steel autoclave for heating for 6 h), here the reaction mixture was poured into a 30 mL microwave synthesis reactor (Monowave 200) vessel and irradiated with microwave at a temperature of 180 °C for 5 min. The colorless solution was converted into a brown color, which showed a bright green fluorescence under UV light (365 nm). The pH of the dispersion was adjusted to 7. The final product was filtered through a 0.22 μm syringe filter to purify the carbon dots and kept at 4 °C temperature for further use. The concentration of the final carbon dot dispersion was 10^{-3} M. So, this modified method could produce carbon dots within 5 min, which generally took 6 h in the case with the use of an autoclave. Hence, it is one of the novel and efficient ways to prepare PEICD.

Preparation of the polyethylene glycol carbon dot (PEGCD, with –OH functional group)

The synthesis of the polyethylene glycol carbon dot (PEGCD) was based on a report given by Gogoi *et al.* with a slight modification.[38] Typically, 0.1 g polyethylene glycol 6000 was taken into a small glass beaker and heated at 180 °C for 1 h through pyrolysis. With time, the color of the solution was changed from colorless to brown, indicating the formation of PEGCD. The resultant solution was mixed with 10 mL water and sonicated for 30 min in a bath sonicator. It was filtered through a 0.22 μm syringe filter to obtain the purified polyethylene glycol carbon dots. The green fluorescence of the dispersion under UV light (365 nm) was additional evidence of the successful formation of PEGCD. The pH of the carbon dot dispersion was at pH 7, neutralized from pH 4 using an ammonia solution with a concentration of around 10^{-2} M and kept at 4 °C temperature for further use.

Preparation of the protein (BSA)-coated polyethylene glycol carbon dot (PEGCD BSA)

The simplest way to make the protein (bovine serum albumin, BSA)-coated polyethylene glycol carbon dot (PEGCD BSA) was to prepare the polyethylene glycol carbon dot and BSA solution separately and mix them in a particular concentration. PEGCD was prepared as discussed above, employing simple pyrolysis. The concentration of the stock PEGCD dispersion (pH 7) was around 10^{-2} M and a particular volume of BSA (10^{-5} M, 2 mg mL^{-1}) was made. Now, to prepare the BSA-coated PEGCD, 2 mL BSA solution was taken and the addition of a particular volume of PEGCD (pH 7, 10^{-2} M) was carried out to monitor the change in the PL spectra of BSA at $\lambda_{em} = 336$ nm (when excited at $\lambda_{ex} = 290$ nm), keeping the mixture undisturbed for 2–3 min after each addition. The gradual decrease in PL intensity of BSA was the indication of the formation of BSA-coated PEGCD. The final volume of the PEGCD BSA dispersion had a carbon dot concentration of approx. 10^{-3} M and the pH was also near 7. The PL quenching behavior during preparation has been included in ESI (Fig. S4†). It was collected and stored at 4 °C temperature for further use.

Interaction of the phosphatidylcholine vesicles (PHOS VES) and carbon dots (CACD, PEICD, PEGCD and PEGCD BSA)

To investigate the possible interaction of carbon dots of varying functionality with the phospholipid vesicles (to act as a model cell membrane), different spectroscopic techniques are employed and the complete methods of study for each carbon dots have been discussed below.

UV-VIS experiment. To investigate the interaction of phospholipid vesicles (PHOS VES) and carbon dots using a UV-Vis spectrophotometer, a 2 mL dispersion (10^{-4} M) of PHOS VES was taken in a 25 mL glass beaker for each carbon dot separately, making a total of four sets. Then, CACD (10^{-4} M), PEICD (10^{-4} M), PEGCD (10^{-3} M) and PEGCD BSA (10^{-3} M) dispersions were prepared in water maintaining pH 7, and added to the respective vesicles in a particular volume in certain time intervals. The resultant dispersion was mixed with a micropipette and kept undisturbed for 2 min. The UV-Vis spectra were recorded for each of the mixtures. The addition of CACD and PEICD was continued until it achieved a concentration of 10^{-5} M in the final mixture for each, whereas a maximum 10^{-4} M concentration was kept for PEGCD and PEGCD BSA. For each case, the change in the spectrum was monitored. The measurements were done in triplicate.

PL experiment. In this experiment, 2 mL of each of the carbon dots, citric acid carbon dot (CACD, 10^{-4} M), polyethyleneimine carbon dot (PEICD, 10^{-4} M), polyethylene glycol carbon dot (PEGCD, 10^{-3} M) and BSA coated polyethylene glycol carbon dot (PEGCD BSA, 10^{-3} M), having pH 7 were taken in a beaker and the respective PL spectra were recorded initially for CACD ($\lambda_{em} = 425$ nm when $\lambda_{ex} = 310$ nm), PEICD ($\lambda_{em} = 465$ nm when $\lambda_{ex} = 340$ nm), PEGCD ($\lambda_{em} = 460$ nm when $\lambda_{ex} = 370$ nm) and PEGCD BSA ($\lambda_{em} = 460$ nm when $\lambda_{ex} = 370$ nm). Then, PHOS VES (10^{-4} M) was added to the carbon dot dispersions and the quenching behavior of the original PL emission peak was observed for each case. The measurements were done in triplicate.

Dynamic light scattering measurement (zeta potential). In this experiment, 2 mL PHOS VES (10^{-4} M) was taken and the

zeta potential was measured in the DLS instrument. Similarly, CACD (10^{-4} M), PEICD (10^{-4} M), PEGCD (10^{-3} M) and PEGCD BSA (10^{-3} M) were each added to PHOS VES, and the zeta potential was recorded after each addition. The process was continued until the 10^{-5} M concentration (for CACD and PEICD) and 10^{-4} M concentration (for PEGCD and PEGCD BSA) were attained in the final mixture, at which a saturation value of the surface charge was obtained for each. Each measurement was done in triplicate.

QCM (quartz crystal microbalance). QCM has been established in many reports so far to get a clear understanding of the probability of interaction of two materials.[39] It has one quartz crystal coated with gold having two electrodes connected with it, and the crystal possesses a fixed resonance frequency, which can change its value with adsorption on it. The Sauerbrey equation (formulated in the year 1959) is the main equation of the QCM technique, which correlates a decrease in the resonance frequency on the quartz crystal (f) with the adsorbed mass (m).[40] The Sauerbrey equation can be represented as:

$$m = C\Delta f / z$$

Here, C (mass sensitivity constant) $= -17 \times 7$ ng (cm^{-2} Hz^{-1}) for a 5 MHz fundamental mode of the quartz crystal, and $z = 1$ is the overtone number.

The equation provides a frequency change (Δf), which in turn gives a mass change (Δm) if one material has affinity for another material on the surface of the quartz plate attached with the instrument. Otherwise, it does not show any variation. Like the previous techniques, here also, four main experiments were performed along with the respective blank experiment. First, the quartz crystal was placed on the specific holder and the instrument was switched on, and kept undisturbed to achieve an approximately constant resistance (R) value (or frequency). Then, 10 μL of PHOS VES (10^{-4} M) was put on the middle portion of the crystal with a micropipette and left for some time so that again, a constant resistance value was attained. A volume of the carbon dots with concentrations of 10^{-4} M (CACD and PEICD) and 10^{-3} M (PEGCD and PEGCD BSA), equivalent to the addition in the case of the UV-Vis, PL and zeta potential measurements with respect to the carbon dots in 10 μL of PHOS VES maintaining a final concentration of 10^{-5} M (CACD and PEICD) and 10^{-4} M (PEGCD and PEGCD BSA), was added on the earlier drop on the crystal. If any interaction of both materials takes place, the Δf and Δm values will automatically come from which extent of interaction can be determined. A maximum of 40 μL of each carbon dot was added beyond the required amount to observe the net change.

Isothermal titration calorimetry (ITC). ITC was used for the study of ligand binding to proteins/nucleic acids and molecular adsorption by polymeric surfaces.[41] It provides the thermodynamic parameters, mainly the binding constant, Gibb's free energy change (ΔG), the enthalpy change (ΔH) and the entropy change (ΔS) when two materials interact.[42] Two methods of titration are normally employed in ITC to study the binding affinity of the liposome and other molecules, like a drug. Type-A titration involves the addition of a solution of a drug/material through a syringe into a cell having a liposome suspension. In contrast, the type-B titration is reversed, putting the liposome suspension in the syringe and injecting it into a drug solution in the cell. The ratio of the number of bound materials and the number of liposomes increases at the end of type-A titration, which may disturb the liposome structure or interaction. This effect can be minimized by the controlled addition. In the case of the type-B titration, the adhesion of the materials onto the liposome is less with respect to the liposomes near the end of the titration, which keeps the vesicles' structure intact. Finally, the whole process of titration is transformed into an equation in terms of the heat flow relating to the injected liposome concentration, and all of the binding parameters are evaluated.[43] Here, ITC was utilized to estimate the binding affinity of the carbon dots of varied functionalities and vesicles working as a model cell membrane. MicroCal iTC$_{200}$ instrument and type-A titration were employed for the ITC experiments, as we could not observe a good binding curve for the type-B titration.[44]

The ITC experiments were performed by taking the equivalent concentrations of both materials (PHOS VES and carbon dots) in each of the four systems, maintained on the basis of the instrument's sensitivity. The stock PHOS VES suspension (0.1 mM) was turbid. Hence, a dilution was done to make the operating concentrations of 0.0048 mM (for PHOS VES CACD), 0.01 mM (for PHOS VES PEICD), 0.066 mM (for PHOS VES PEGCD) and 0.008 mM (for PHOS VES PEGCD BSA) to put in the ITC cell. In order to maintain the carbon dots concentration in each case, a respective dilution was applied from the original dispersion to make a concentration of 0.066 mM (for CACD and PEICD) and 0.66 mM (for PEGCD and PEGCD BSA) to be kept in the syringe. Typically, 38 μL of carbon dots dispersion having the concentrations mentioned above was injected with 0.4 μL (first injection) and 2 μL (the subsequent seventeenth injections) into 280 μL of PHOS VES in the cell with a 500 rpm stirring speed at 28 °C. The injectant was added at certain intervals (3 min) so that the titration peak returned to the baseline before each injection. Water was used in the reference cell of the instrument. The reference power of 5 was maintained in the instrument. A one-site model was employed to get the binding isotherm.

Linear sweep voltammetry (LSV). The electrochemical technique is also an important method of studying the interaction of two materials. In particular, we have employed the linear sweep voltammetry (LSV) experiment, considering potassium chloride (KCl) as the main supporting electrolyte with a co-electrolyte, and potassium ferricyanide ($K_3[Fe(CN)_6]$) to attain a prominent anodic stripping peak current.[45] 10 mL KCl (0.1 M) and 1 mL $K_3[Fe(CN)_6]$ (0.1 M) were mixed to prepare the supporting electrolyte. A potential range of -0.45 V to 1.45 V was applied with a scanning rate of 100 mV s^{-1} in the three-electrode system. Glassy carbon was taken as the working electrode, Ag$^+$/AgCl as the reference one and platinum as the counter electrode. The experiments were performed with the glassy carbon electrode, deposited with PHOS VES and PHOS VES PEICD. Then, the parameters were set by inserting the three electrodes into the electrolyte system to explore the current change with respect to the potential.

Instrumentation techniques. Various spectroscopic techniques were employed to characterize the synthesized materials. The Shimadzu UV-VIS Spectrophotometer, UV-2600 was utilized to record all of the relevant UV-Vis spectra. A Jasco spectrofluorometer (FP-8300) was used to obtain the fluorescence spectra for the carbon dots and the corresponding interaction study with vesicles. Dynamic light scattering (DLS) size and zeta potential for all of the particles were evaluated on a Malvern Zetasizer Nano series, Nano-ZS90. The mass change and frequency change coming from the interaction study were measured in a Quartz Crystal Microbalance machine (SRS, Model: QCM200). The particle structure and morphology were captured in a transmission electron microscope (TEM-2100 Plus, JEOL). The lifetime and decay profile of the samples were found in a time-resolved photoluminescence spectrometer (EDINBURGH INSTRUMENTS, Model: LifeSpec II). Functional groups present were identified by Fourier transform infrared spectra using a Nicolet-6700 FTIR spectrophotometer. The fluorescence intensity of the prepared carbon dots under UV light (365 nm) was observed in a JSGW UV lamp.

Results and discussion

In this study, we attempted to study the interaction at the interface of cell with carbon-based nanomaterials. In this study, vesicles th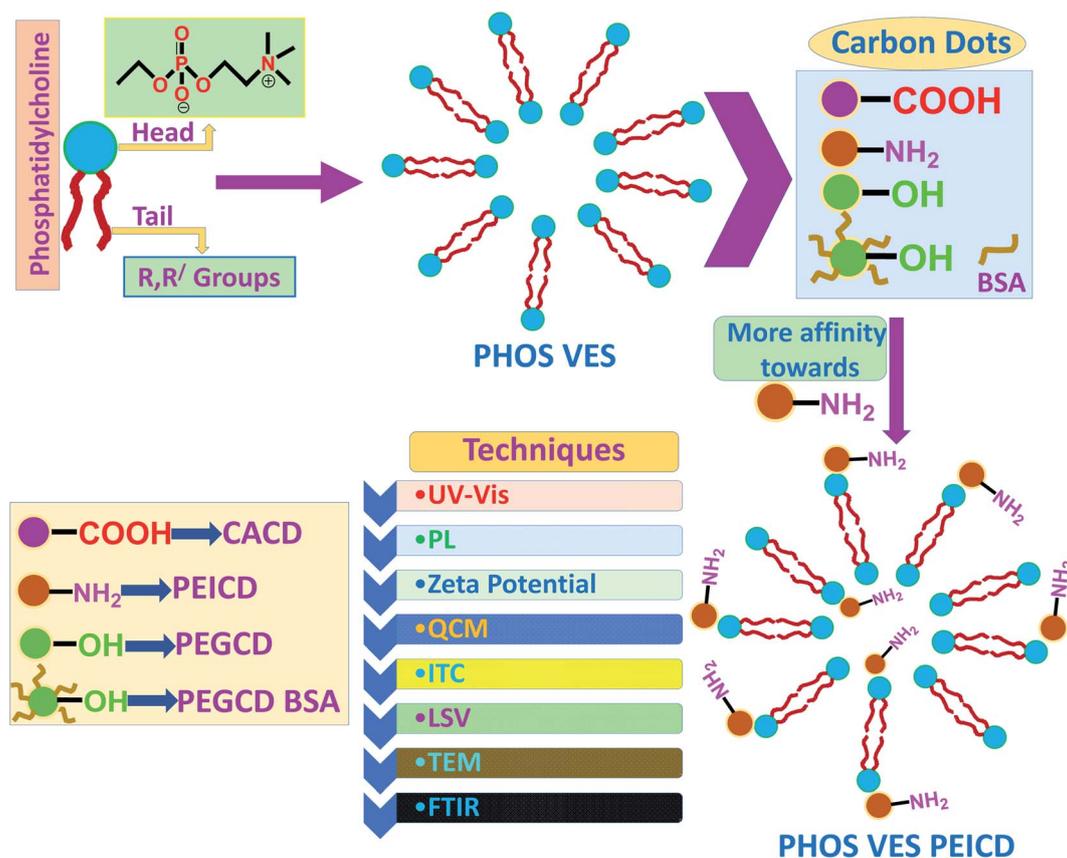at resemble our cell membrane (owing to its composition and structure) were taken as a model system. For the carbon nanomaterials with different terminal functionalities on its surface, their impact on the cell membrane might be altered depending on the functional groups. However, the affinity of a nanoparticle towards the cell structure might have dependency on its functional groups. Hence, to study this aspect, we prepared four different carbon dots having functionality –COOH, –NH$_2$, –OH, protein-coated and one phosphatidylcholine vesicles system to be used as the model cell membrane, and finally attempted to investigate the probable interaction with individual carbon quantum dots with the vesicles. The number of spectroscopic (UV-Vis, PL, DLS, FTIR, QCM, ITC, LSV) and microscopic (TEM) techniques were used to understand the possible interaction of the functionalized carbon nanomaterials with the vesicles. Scheme 1 represents the flow chart showing the protocol that was followed in the experiment, including the fabrication of the phosphatidylcholine vesicle system (PHOS VES), the four different carbon dots with different functionality, and the different techniques used to study the interaction. The detailed synthetic protocol adopted for each preparation and synthesis is discussed in the experimental section above.

Characterization of the phosphatidylcholine vesicles (PHOS VES)

The phosphatidylcholine vesicles (PHOS VES) were prepared by film hydration method (details in the Experimental section).

Scheme 1 Flowchart showing the formation of PHOS VES, followed by interaction of four different carbon dots with different functional groups (CACD, PEICD, PEGCD and PEGCD BSA).
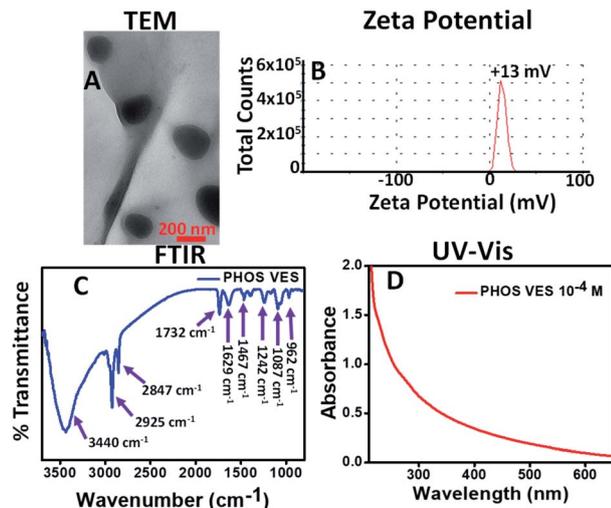
Fig. 1 (A) TEM image, (B) zeta potential, (C) FTIR spectrum, and (D) UV-Vis spectrum of PHOS VES (aqueous medium is used as blank).

The PHOS VES was subjected to various characterization techniques. The PHOS VES was visualized using transmission electron microscopy (TEM). The TEM image shows that PHOS VES is almost spherical in shape with the size around 200 nm, as shown in Fig. 1A.

The surface charge on the PHOS VES was also measured in terms of the zeta potential, and was determined to be $\zeta = $ +13 mV as shown in Fig. 1B. The positive ζ is due to the presence of the tertiary nitrogen and partial positive charge on the phosphorous present in the head group. The FTIR spectrum for PHOS VES was also recorded, and is shown in Fig. 1C below. It possesses mainly C–H stretching vibration (2925 and 2847 cm^{-1}) along with the O–H stretching vibration (3428 cm^{-1}), which may come from the residual solvent water. There is another vibration near 1732 cm^{-1}, which is due to the carbonyl group (–O–C=O) in the tail part of the phospholipid. The peak near 1629 cm^{-1} appears from the C=C functionality present on the phospholipids' tail group (alkyl chain). The other FTIR peak (1467 cm^{-1}) reveals the presence of the C–H bending vibration. Furthermore, the peak near 1242 cm^{-1} signifies the presence of the –P=O vibration. The peaks at 1087 and 962 cm^{-1} correspond to the –P–O_{asym} and –P–O_{sym} stretching vibrations present in the head group of the phospholipid molecules.[46] Finally, the UV-Visible spectrum of the vesicles was taken, as shown in Fig. 1D. It implies that the maximum absorption peak (though very weak) appears near 270 nm.

Characterization of four different carbon dots (CACD, PEICD, PEGCD and PEGCD BSA)

In this study, the four different carbon dots, CACD, PEICD, PEGCD and PEGCD BSA, were prepared as per the experimental protocol described. All of the prepared carbon dots, as described above, were subjected to various spectroscopic and microscopic techniques, like dynamic light scattering (DLS) analysis, transmission electron microscopy (TEM), UV-Visible spectroscopy, photoluminescence (PL), FTIR, and time-

resolved photoluminescence (TRPL) spectroscopy. Fig. S1 in ESI† depicts the various characterizations done on CACD with a detailed discussion. Similarly, the characterization studies along with its discussion of the other synthesized carbon dots, *viz.*, PEICD, PEGCD and PEGCD BSA, can be found in Fig. S2, S3 and S5, respectively, in ESI.†

Interaction studies of phosphatidylcholine vesicles and citric acid carbon dots (PHOS VES–CACD)

To study the interaction of the phosphatidylcholine vesicles and citric acid carbon dots bearing the –COOH functional group, various techniques (like UV-Visible spectroscopy, photoluminescence spectroscopy, zeta potential study and quartz microbalance study) were utilized. The UV-visible study was done by adding the CACD solution dropwise to the vesicles solution and monitoring the spectrum. The observed UV-visible spectrum is shown in Fig. S6A in ESI.† It is evident from the spectrum that PHOS VES has no peak near 335 nm (black). However, when CACD is added, no significant change was observed in the absorption spectrum. However, an excess of CACD results in the emergence of the 335 nm peak (blue curve), which is the characteristics of the n–π* transition of CACD when compared with the UV-Visible spectrum of CACD (Fig. S1D, ESI†). This observation clearly shows that there is no observed interaction between the phosphatidylcholine vesicles and citric acid carbon dots.

As CACDs are fluorescent, the photoluminescence property of CACD can be utilized to study the interaction of the phosphatidylcholine vesicles and citric acid carbon dots (CACDs). In this study, the effect of the PL properties of CACD was monitored to follow the interaction of the vesicles. As discussed before, CACD shows a maximum PL emission at 425 nm at 310 nm excitation. It was observed that there was no change in the PL intensity of CACD at 425 nm (Fig. S1E, ESI†) in the presence of the phosphatidylcholine vesicles. Whatever negligible change was observed was only due to dilution. Fig. S6B† shows the histogram of change of the PL intensity after the addition of the phosphatidylcholine vesicles. Hence, it can be concluded that there is no change in the PL property of CACD when interacting with the phosphatidylcholine vesicles (PHOS VES).

The surface charge on the vesicles may greatly affect the interaction, and may provide valuable information of the possible interaction of the phosphatidylcholine vesicles in the presence of CACD. So, the surface charge on the phosphatidylcholine vesicles was studied in the presence of CACD by measuring the zeta potential (ζ). PHOS VES has a zeta potential value of +13 mV and CACD has a value of −16 mV. When the negative carbon dot (10^{-4} M) is added gradually in a small amount to PHOS VES, the positive potential slowly changes to zero and then becomes negative. After a particular volume of CACD is added, the zeta potential attains a constant value of approximately −28 mV. The change in the zeta potential value of PHOS VES on the successive addition of CACD is shown in Fig. S6C.† The trend shows that on addition of negatively charged CACD to positively charged PHOS VES, a charge

neutralization initially takes place. With excess CACD, a negative potential then persists in the final mixture (CACD concentration 10^{-5} M) and a saturation value was ultimately achieved.

Another technique that can be really useful to study the interaction of the phosphatidylcholine vesicles and carbon dots is the Quartz Crystal Microbalance. The Quartz Crystal Microbalance (QCM) is an extremely sensitive mass balance that measures nanogram/level changes in mass per unit area. The change of frequency of oscillation of the crystal can be monitored in real time to obtain useful information about molecular interactions. So, a QCM experiment was done to study the interaction of PHOS VES and CACD, and is shown in Fig. S6D.† Maintaining an equal concentration of the PHOS VES and CACD (as in UV-Vis, PL, zeta potential), QCM analysis was performed. QCM provides Δm in µg cm^{-2} unit. With increasing Δm, there will be more adsorption (or interaction). From the plot, it was observed that on addition of 10 µL of PHOS VES on the quartz crystal at the beginning, a sudden increase in Δm takes place, signifying the strong adsorption of vesicles on the crystal. Then, a small addition of CACD onto the PHOS VES drop was carried out, which is equivalent to the final concentration of carbon dots in all three experiments above. A blank experiment was performed with the same volume of water, and denoted as PHOS VES WATER. It was found that Δm is lesser for PHOS VES CACD (5.759 µg cm^{-2}) than the blank experiment (7.331 µg cm^{-2}), confirming the fact that no observable adsorption of CACD on the PHOS VES occurred. The pure CACD has a Δm value of -1.572 µg cm^{-2}. The addition of CACD was continued beyond the equivalent concentration, but no further change was observed.

The ITC results revealed that on titration of PHOS VES with CACD, the heat flow/change that took place with respect to time was almost constant during the complete period of titration, as shown in Fig. S6E in ESI,† which indicates no such strong binding of the two materials. In fact, the heat produced for each injectant was obtained to be abrupt and did not fit to a smooth curve (Fig. S6F†), leading to a similar prediction. The dissociation constant, K_d, and enthalpy change, ΔH, for the complete titration were found to be 1.53 µM and $(-5.79 \times 10^7) \pm (1.94 \times 10^{12})$ kcal mol^{-1}, as put in the inset of Fig. S6F.†

Interaction of phosphatidylcholine vesicles and polyethyleneimine carbon dots (PHOS VES PEICD)

Similar studies were conducted to study the interaction between the phosphatidylcholine vesicles and polyethyleneimine carbon dots bearing the –NH$_2$ functional group. The UV-Vis study was performed as shown in Fig. 2A. It was observed that when PEICD was added to PHOS VES, the peak of PEICD at 360 nm arising due to the n–π* transition started to appear.

A PL study was also carried out to study the PL behavior. The PL spectra were recorded for PEICD in the presence of PHOS VES. PHOS VES (10^{-4} M) was added to PEICD (10^{-4} M) as described, maintaining the concentration of PEICD at 10^{-5} M at the final stage. Interestingly, the PL intensity of PEICD at the 465 nm peak (Fig. S2E, ESI†) got significantly quenched on

addition with PHOS VES. The bar diagram (Fig. 2B) clearly compares the change of the fluorescence intensity, and the probable interaction of both systems can be inferred.

The surface charge change of PHOS VES on addition of PEICD was monitored by measuring the zeta potential value, and the relevant plot is shown in Fig. 2C. It needs to be noted that PHOS VES has a zeta potential value of +13 mV and PEICD has a value of +36 mV. When the carbon dots (10^{-4} M) were added gradually in small amounts to PHOS VES, the positive potential of the vesicles suddenly achieved a higher positive value of around +36 mV and then remained constant at a PEICD concentration of 10^{-5} M in the final volume. In spite of the positive potential on both systems, the affinity of the amine group towards the cell surface may be the driving force to attract each other. The affinity of vesicles towards the amine group has been observed in the case of the neurotransmitter vesicular transportation in neurons.[47] The immediate potential change can be interpreted in terms of the attachment of PEICD onto the surface of vesicles. The constant zeta potential value indicates the saturation point.
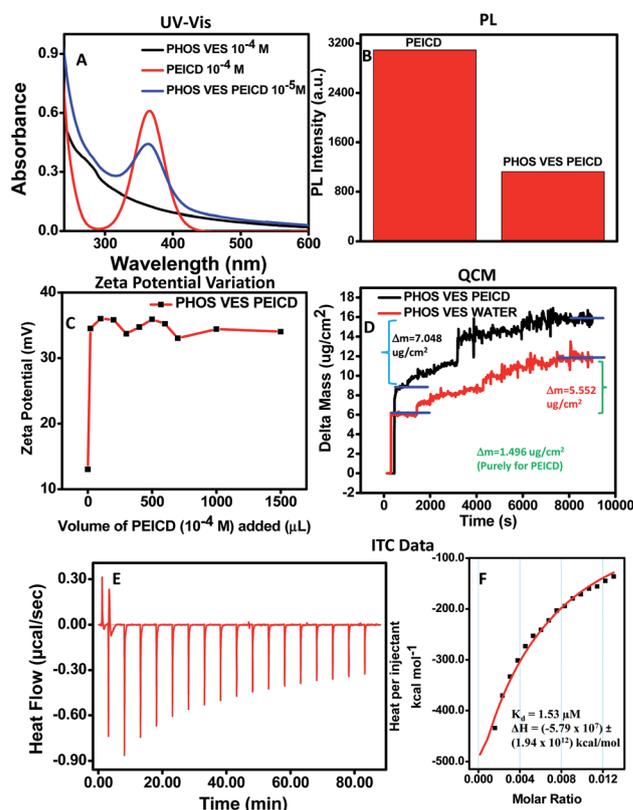

Fig. 2 Experiment of (A) change of the UV-Vis spectra of PHOS VES (10^{-4} M) with the addition of PEICD (10^{-4} M), and (B) change of the PL intensity of PEICD (10^{-4} M) with the addition of PHOS VES (10^{-4} M). (C) Change of the Zeta Potential of PHOS VES (10^{-4} M) with the addition of PEICD (10^{-4} M). (D) Change of the mass (m)/frequency (f) of PHOS VES (10^{-4} M) with the addition of PEICD (10^{-4} M) in QCM. (E) Heat flow/change vs. time plot, and (F) heat produced per injectant with the rise in the molar ratio of the two materials in ITC measurements. The inset of Fig. 2F shows the dissociation constant, K_d, and enthalpy change, ΔH, for the titration (aqueous medium is used as the blank).

A QCM experiment was also carried out to study the interaction between the phosphatidylcholine vesicles and polyethyleneimine carbon dots. From the plot (Fig. 2D), it was obvious that the addition of 10 mL of PHOS VES on the quartz crystal shows higher Δm as in the earlier case. Then, PEICD was added to the PHOS VES drop in an equivalent concentration, as in all three experiments above. A blank experiment was also carried out. Surprisingly, Δm was much higher for PHOS VES PEICD (7.048 µg cm^{-2}) than the blank experiment (5.552 µg cm^{-2}), indicating the significant adsorption of the carbon dots on the PHOS VES. Δm was found to be 1.496 µg cm^{-2} for pure PEICD. The addition of carbon dots was continued beyond the equivalent concentration, but no further change was observed.

ITC experiments were successful in revealing the stronger binding for PHOS VES with PEICD. Fig. 2E represents the heat flow/change occurring with time when PHOS VES is titrated with PEICD. It showed that initially, a large heat change was observed up to a certain addition of PEICD and then gradually got a stable value (60 min onwards), indicating the saturation. Strong binding of the two materials was prominent from this plot. Meanwhile, the heat produced for each step of the titration was gradually decreased and fitted to a smooth curve (Fig. 2F), leading to the fact that titration tends to develop a stable form with combining the two materials. The exothermic nature of heat flow for the binding of PHOS VES and PEICD could be interpreted from the value of the released (negative) heat in Fig. 2F. The reduction of heat release may be described by the fact that on addition of more PEICD to vesicles, PHOS VES is covered with PEICD, limiting the number of free vesicles.[44] The dissociation constant, K_d, and enthalpy change, ΔH, were also determined and are shown in the inset of Fig. 2F. For the complete titration, K_d and ΔH were calculated to be 1.53 µM and $(-5.79 \times 10^7) \pm (1.94 \times 10^{12})$ kcal mol^{-1}, respectively.

The greater binding ability of PEICD towards PHOS VES, resulting in a composite system, was also investigated with LSV, as shown in Fig. 3A. From the plot, it was observed that the supporting electrolyte with the glassy carbon electrode deposited with PHOS VES could detect the anodic stripping peak current of 1.47×10^{-5} A when the potential was 0.17 V. However, on deposition of the PHOS VES PEICD on the working electrode, the anodic stripping peak current changed significantly to 1.24×10^{-4} A at a potential of 0.14 V. Moreover, the slightly shifted peak position in the LSV plot may infer the

formation of PHOS VES PEICD by interacting with the vesicles and PEICD.

Time-resolved photoluminescence (TRPL) spectra were also taken to investigate the interaction of PHOS and PEICD. As predicted from the discussion in Fig. 2B, the PL properties were clearly indicative of the quenching due to the attachment of PEICD onto the vesicles, so we further wanted to study the respective decay profile and lifetime calculation for this particular system (PHOS VES PEICD) in the TRPL instrument (using EPLED-295), as done in the carbon dots characterization. The obtained result is shown in Fig. 3B. No change in the decay profile for PEICD and PHOS VES PEICD was observed. But, slight difference in their lifetime (τ) was found. PEICD had lifetime values of 1, 4.03, and 9.91 ns, while PHOS VES PEICD had values of 0.92, 3.66, and 9.36 ns. The TRPL data show that the decay profiles of PEICD and PHOS VES PEICD are similar.

Interaction of the phosphatidylcholine vesicles and polyethylene glycol carbon dots (PHOS VES PEGCD)

A similar study was performed to study the interaction of the phosphatidylcholine vesicles and polyethylene glycol carbon dots (PEGCD) bearing the –OH functional group. The UV-Vis experiment results are presented in Fig. S7A in ESI† when PEGCD is added to PHOS-VES. It was observed that there is no observable change in the UV-Vis spectrum detected when PEGCD is introduced to PHOS VES.

The PL study was also conducted to study the PL behavior of PEGCD in the presence of PHOS VES. The PL intensity at 460 nm emission of PEGCD (10^{-3} M) was monitored (Fig. S3E, ESI†). It was observed that there is no notable change in the PL intensity at 460 nm emission when PHOS VES is introduced to PEGCD. The bar diagram (Fig. S7B†) clearly shows the change of the PL intensity.

The surface charge determined by measuring the zeta potential of PHOS VES on addition of PEGCD is shown in Fig. S7C.† Here, the PHOS VES has a zeta potential value of +13 mV and PEGCD has a value of −16 mV. The zeta potential value gradually changes from positive to negative when carbon dots (10^{-3} M) are added gradually in small amounts to PHOS VES, and finally gets a constant value around −6 mV due to reaching the saturation point. The trend is linked with the charge neutralization of the systems in the mixture. A PEGCD concentration of 10^{-4} M was maintained in the final volume. The gradual change of the potential came from adding a negatively charged material to a positively charged material.

The QCM experiment done to study the interaction of the phosphatidylcholine vesicles and polyethylene glycol carbon dots is shown in Fig. S7D.† The plot shows that the addition of 10 µL of PHOS VES on the quartz crystal showed higher Δm as in an earlier case. Then, PEGCD was added onto the PHOS VES drop at an equivalent concentration as in all three experiments above. A blank experiment was also carried out. It was found that Δm is higher for PHOS VES PEGCD (7.422 µg cm^{-2}) than the blank experiment (6.193 µg cm^{-2}). Δm was found to be 1.229 µg cm^{-2} for pure PEGCD, which is comparatively less than PEICD (1.496 µg cm^{-2}).
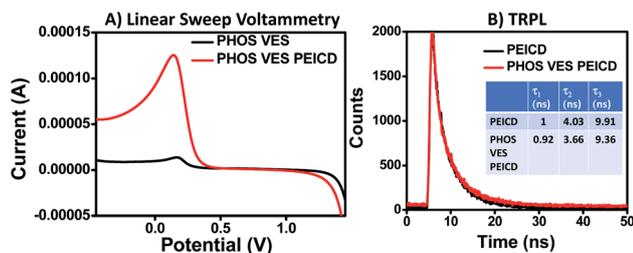

Fig. 3 (A) Linear sweep voltammetry data. (B) Comparative fluorescence decay pattern and lifetime (τ) of PEICD (10^{-4} M) and PHOS VES PEICD.

Similar to the ITC data of PHOS VES CACD, on titration of PHOS VES with PEGCD, the heat flow/change was measured to be nearly constant for the whole span of injection of PEGCD onto PHOS VES, as represented in Fig. S7E in ESI.† It implies that there was no significant binding affinity of the two materials towards each other. Furthermore, for each addition of injectant, the heat produced was not in a trend, but rather scattered (Fig. S7F†), deviating from the fitting curve. The thermodynamic parameters, like the dissociation constant, K_d and enthalpy change, and ΔH, were evaluated for the complete titration and found to be 18.1 µM and $(-9.14 \times 10^4) \pm (5.38 \times 10^{10})$ kcal mol^{-1}, respectively (inset of Fig. S7F†).

Interaction of phosphatidylcholine vesicles and BSA-coated polyethylene glycol carbon dots (PHOS VES PEGCD BSA)

The final system that was studied was the interaction of phosphatidylcholine vesicles and BSA-coated polyethylene glycol carbon dots (PHOS VES PEGCD BSA). In this system, the carbon dots were not bare like CACD, PEICD and PEGCD. Instead, it was coated with a protein BSA. The UV-Vis experiment of PHOS VES in the presence of the BSA-coated PEGCD is shown in Fig. S8A.† It is evident from the UV-Vis spectrum that PHOS VES shows a weak peak near 270 nm (black curve) and PEGCD BSA shows two peaks, one near 225 nm and the other one at 280 nm (red curve). When the BSA-coated PEGCD carbon dot was added, the original vesicle spectrum displayed one additional peak at 280 nm, which obviously comes from PEGCD BSA (blue curve). The final concentration of the PEGCD BSA in the mixture was recorded to be 10^{-4} M. There is no change in the spectrum, except the addition band in the presence of carbon dots in the mixture.

The PL property was studied to investigate the possible interaction between PHOS VES and BSA-coated PEGCD, as shown in Fig. S8B.† The PL emission at 465 nm (Fig. S5E, ESI†) was monitored when PHOS VES (10^{-4} M) was added to PEGCD BSA (10^{-3} M). The concentration of PEGCD BSA was maintained at 10^{-4} M at the final stage. It was observed that there is no change in the PL intensity when vesicles are added to BSA-coated PEGCD as shown in the bar diagram.

The zeta potential change for the addition of PEGCD BSA in PHOS VES was monitored, and the data are shown in Fig. S8C.† PEGCD BSA has a surface charge value of −11 mV. On addition of carbon dots (10^{-3} M) into the vesicles (10^{-4} M), the positive zeta potential of PHOS VES gradually changes from positive to negative, and finally remains constant around −4 mV due to reaching the saturation point. The process follows the charge neutralization of the two systems in the mixture rather than interaction, as explained in case PEGCD. The concentration of PEGCD BSA is maintained at 10^{-4} M in the final volume.

A QCM experiment performed to study the interaction of PHOS VES and PEGCD BSA is shown in Fig. S8D.† As found earlier, here too, the addition of 10 mL of PHOS VES on the quartz crystal showed high Δm. PEGCD BSA (10^{-3} M) was added onto the PHOS VES (10^{-4} M) drop at an equivalent concentration with respect to the previous experiment, and the obtained Δm value was compared with the blank experiment. It was found that Δm is higher for PHOS VES PEGCD BSA (7.542 µg cm^{-2}) than the blank experiment (6.445 µg cm^{-2}). In fact, Δm (purely for PEGCD BSA) was found to be 1.097 µg cm^{-2}. The data do not reflect the strong interaction between PHOS VES and the BSA-coated PEG.

In the case of the ITC experiment for the titration of PHOS VES with PEGCD BSA, a similar observation was noticed as that for CACD and PEGCD. Fig. S8E in ESI† shows that there was no significant heat flow/change when PEGCD BSA was added to the vesicles until the end of the titration. Weak binding affinity of the two materials towards each other can be explained with this plot. However, the scattered heat released or absorbed during the injection appearing in Fig. S8F† leads to the instability, which is related to the lesser binding effect. Also, the dissociation constant, K_d, and enthalpy change, ΔH, were mentioned in the inset of Fig. S8F.† Both were measured to be 2.5 µM and $(-26.13) \pm (6.52 \times 10^2)$ kcal mol^{-1}, respectively.

Transmission electron microscope (TEM) analysis

Transmission electron microscopy technique was utilized to visually determine any possible interaction between PHOS VES and all of the different functionalized carbon dots, CACD, PEICD, PEGCD and BSA-coated PEGCD. PHOS VES was allowed to interact with the carbon dots and viewed under an electron microscope. Fig. 4A(1–4) represent representative TEM images of PHOS VES CACD, PHOS VES PEICD, PHOS VES PEGCD and PHOS VES PEGCD BSA. The collected images clearly show that circular vesicles are visible, and the carbon dots as tiny dots could also be detected from the images. Fig. 4A(2) shows the TEM for PHOS VES PEICD. Interestingly, here, the spherical vesicles of size around 200 nm are surrounded by some black dots, which are actually carbon dots. A majority of the carbon dots seem to be in affinity of PHOS VES. We believe this is direct visual evidence for demonstrating the affinity of PEICD towards PHOS VES. Other systems PHOS VES CACD, PHOS VES PEGCD, as observed from TEM images, suggest that carbon dots do not have affinity towards the PHOS VES, but are distributed randomly, indicating no interaction. Moreover, the TEM image for PHOS VES PEGCD BSA (Fig. 4A(4)) shows no carbon dots on the vesicles surface.

Rather, a deformation of the vesicles takes place. Thus, the TEM image clearly gives direct visual evidence that among the different functionalities present on the carbon quantum dots, PEICD, $-NH_2$ (amine) containing carbon quantum dots possesses grater affinity and more interaction with PHOS VES. It is also supported by QCM and ITC data.

Comparative FTIR spectra analysis

FTIR spectra were recorded for all four carbon dots and the respective resultant systems. Fig. 1C depicts that PHOS VES has mainly $-P-O_{asym}$ and $-P-O_{sym}$ (1087 and 962 cm^{-1}, respectively), $-P=O$ (1242 cm^{-1}), $-C-H$ (2925 and 2847 cm^{-1}) and O–H stretching vibration (3440 cm^{-1}, may be from residual water) along with one at 1732 cm^{-1}, which could be due to $-O-C=O$. Here, the comparative FTIR spectra separately for each carbon dot are included in Fig. 4B and S9(A–C) of ESI.† All four plots

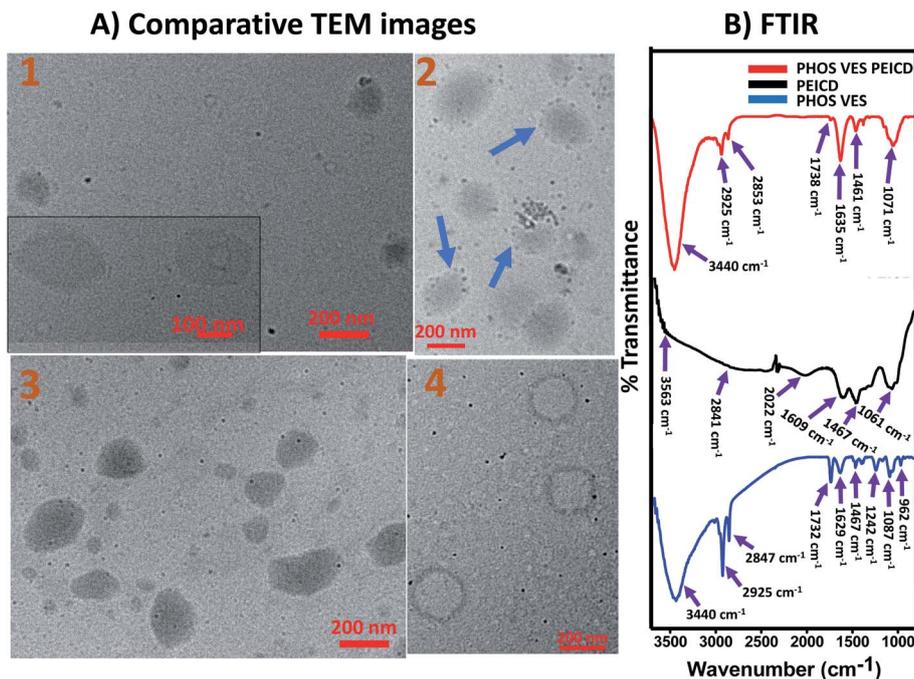## A) Comparative TEM images

B) FTIR

Fig. 4 TEM images of (A1) PHOS VES CACD (high resolution image at the inset), (A2) PHOS VES PEICD, (A3) PHOS VES PEGCD (A4) PHOS VES PEGCD BSA, (B) comparative FTIR spectra of PHOS VES (blue), PEICD (black) and PHOS VES PEICD (red).

have the same FTIR spectrum of PHOS VES for comparative purpose.

PEICD contains –N–H stretching vibration (3563 cm^{-1}), –C–H stretching (2841 cm^{-1}), –C–H bending vibration (2022 and 1467 cm^{-1}), –C–N stretching (1061 cm^{-1}) and –N–H bending and/or –C=N stretching (1609 cm^{-1}), which are prominent (Fig. 4B, black).[37] PHOS VES PEICD has –N–H stretching (3440 cm^{-1}), –C–H stretching (2925 cm^{-1}, 2853 cm^{-1}), –C=C stretching (1635 cm^{-1}) vibrations, as shown in Fig. 4B (red). It was observed that the –C=O present in PHOS VES almost vanished (1738 cm^{-1}) when PEICD was attached, forming PHOS VES PEICD. Furthermore, the peaks for –P–O$_{sym}$ and –P=O (962 cm^{-1} and 1242 cm^{-1}, respectively) present in the PHOS VES head group disappear when PEICD interacted with the vesicles. This indicates the binding of PEICD with the PHOS VES. This observation is also in agreement with the observation inferred from other techniques.

Fig. S9A in ESI† has the FTIR spectrum for CACD (black). It was found that CACD has H-bonded –O–H stretching (3505 cm^{-1}), and –N–H stretching, which comes from the ammonia solution used to adjust the pH of CACD (3138 cm^{-1}), –C=O stretching vibration (1706 cm^{-1}), –C=C stretching vibration (1577 cm^{-1}, which may come from itaconic acid or citraconic acid or *trans*-aconitic acid resulting as an intermediate product during citric acid heating),[36] and the =C–H bending vibration (1396 cm^{-1}). All of those peaks suggest the presence of –COOH functionality on CACD. Now, PHOS VES CACD (red) possesses –O–H stretching (3447 cm^{-1}), –C–H stretching (2925 cm^{-1} and 2853 cm^{-1}), –C=O stretching vibration (very weak, 1732 cm^{-1}), 1622 cm^{-1}, 1383 cm^{-1} and 1067 cm^{-1}, as presented in the same figure. Hence, on

interacting with CACD and PHOS VES, the signature peak for –OH is intact in the final spectrum, which demonstrates no significant interaction between them. In fact, the peaks for –P–O$_{sym}$ and –P=O present in PHOS VES also appeared in the PHOS VES CACD spectrum, confirming very weak interaction of both materials. This is also in agreement with the observation inferred from other techniques.

The functional group present in PEGCD was determined to be –O–H stretching (3401 and 3124 cm^{-1}), –C–H stretching (2918 cm^{-1} and 2873 cm^{-1}), and –C=O stretching (1726 cm^{-1}), which may come from some intermediate product during pyrolysis, –C=C stretching (1616 cm^{-1}), –C–H bending (1396 cm^{-1}), and –C–O stretching (1093 cm^{-1}), as shown in Fig. S9B† (black).[38] However, PHOS VES PEGCD contains –OH stretching (3453 cm^{-1}), –C–H stretching (2925 and 2847 cm^{-1}), –C=C stretching (1635 cm^{-1}), –P=O stretching (1383 cm^{-1}), and –C–O stretching (1067 cm^{-1}) vibrations (red curve, Fig. S9B†). It was noted that on interacting PHOS VES with PEGCD, the –P=O peak is intact as in PHOS VES. So, no prominent binding between the two materials could be revealed from the spectrum. This is also in agreement with the observation inferred from other techniques.

However, Fig. S9C† (black) depicts that PEGCD BSA is found to have –O–H and/or –N–H stretching (3415 and 3111 cm^{-1}), –C–H stretching (2918 and 2860 cm^{-1}), –C=O stretching (1726 cm^{-1}, from amino acid group of protein BSA), –C=C stretching (1648 cm^{-1}), –C–H bending (1390 and 1455 cm^{-1}), and –C–O stretching (1100 cm^{-1}). In PHOS VES PEGCD BSA (red curve, Fig. S9C†), the present vibrations are for –O–H and/or –N–H stretching (3434 cm^{-1}), –C–H stretching (2931 cm^{-1}, 2860 cm^{-1}), –C=O stretching (1732 cm^{-1}), –C=C stretching

(1635 cm^{-1}), –C–H bending (1461 cm^{-1}), –P=O stretching (1396 cm^{-1}), -C–O and/or –P–O$_{asym}$ stretching (1081 cm^{-1}). It indicates that the main probable binding sites –O–H, –P=O and –P–O$_{asym}$ are present, and their respective peak positions are intact. Hence, no clear interactive statement can be inferred from the spectrum. This is also in agreement with the observation inferred from other techniques.

From the above FTIR spectral analysis, it is clear that there is interaction of PHOS VES and PEICD, which is not present with the other functionalized carbon quantum dots, *viz.*, CACD, PEGCD BSA and PEGCD.

Mechanistic insight

The probable mechanism of action for the selectivity of a particular functional group bearing the carbon dots towards the model cell membrane of phospholipid vesicles is shown in Fig. 5. It is apparent that the phospholipid vesicles (PHOS VES) possess two extreme layers (inner and outer) with negative phosphate group and positive substituted quaternary ammonium ion, along with two long chain fatty acid groups inside the two extreme layers. The head group is the reactive sites for the vesicles. The presence of the carboxylic anion on the CACD (due to ammonia used for the pH neutralization of the CACD) has only one attacking site on the head group (positive quaternary ammonium group) of the vesicles, which is hindered by the steric factor. So, no proper interaction takes place with CACD. In fact, in the case of PEGCD, the hydroxyl groups get protonated due to the H^{+} (HCl) ion present (applied for pH adjustment). Hence, the PEGCD only interacted through the substitution reaction by the oxyanions on the phosphate group

to replace water on PEGCD. Finally, no hydroxyl group will be present on the PEGCD. Although very few –O–H groups will be there to react with the head group with weak H-bonding, it is not sufficient to bind strongly with the vesicular wall. However, when BSA is coated onto the PEGCD, the former –O–H group and oxonium ions are trapped by the protein amino acid, which leaves no further site for interaction with the head group in the case of PEGCD BSA. A weak electrostatic attraction was found to be operated between the positive oxonium ion on the BSA-coated PEGCD with the oxyanion on phosphate group. Here also, steric hindrance coming from the protein part is another contributing factor to prevent such strong binding. However, PEICD has a free –NH$_2$ group (owing to the ammonia used for pH adjustment), which facilitates H-bonding from the lone pair and negative ions on the oxygen atom of the phosphate groups towards the two H-atoms of amine group of PEICD. There are four sites on the head group of the vesicles, allowing such strong H-bonding, leading to the sufficient attachment of carbon dots onto the PHOS VES. Among all four carbon dots, the better performance of the amine-terminating carbon dots with stronger binding ability is also supported by some other facts reported earlier. It is noted that the transport of neurotransmitters in neurons for cellular communication through synapse is only possible through vesicular platforms.[48,49] The neurotransmitters are basically amino acid-containing amine and carboxylic functional groups. In fact, such vesicular transporters also carry neurotransmitters having only amine group smoothly.[47] So, it implies the vital role of amine functionality. The cellular communication specially in the central nervous system using vesicles is very much crucial, and the successful
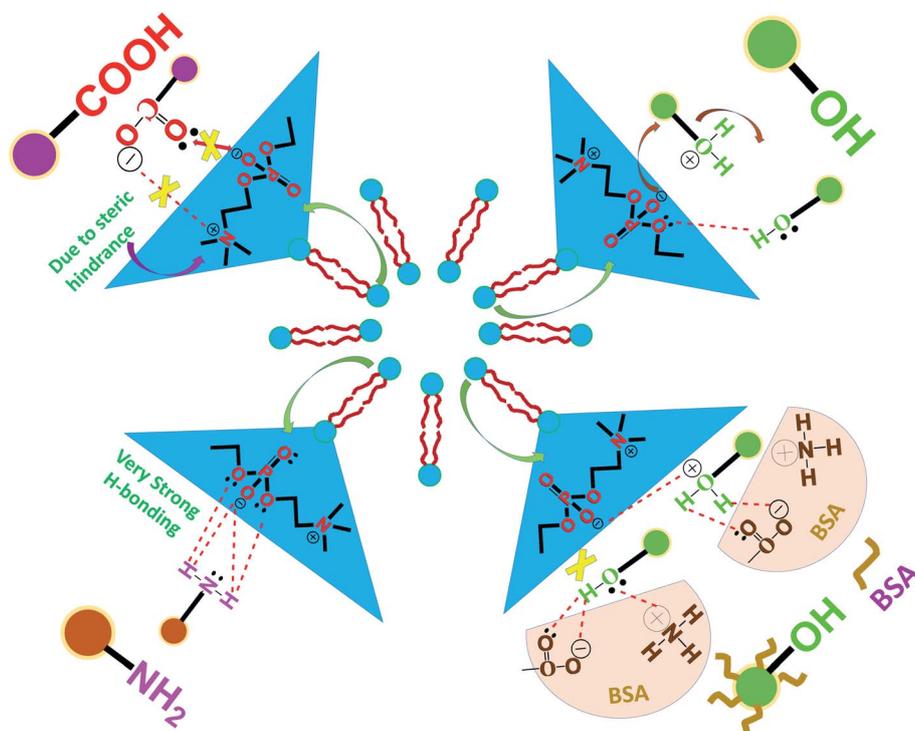

Fig. 5 Schematic representation of the probable mechanism of the interaction of carbon dots with PHOS VES.

interaction of vesicles and molecules with amine functionality has already been established in the case of neurons, which may be applicable to other cells in our body. Furthermore, most of the drugs available in the market for different ailments (*e.g.*, doxorubicin, dacarbazine, paracetamol, cefadroxil chlorpheniramine, chlorpromazine, ephedrine, phenylephrine, amphetamine, methamphetamine, methcathinone, thioridazine, amitriptyline, imipramine, lofepramine and clomipramine, nortriptyline, desipramine, and amoxapine are some of the amine containing drugs) possess the amine functionality, which may be another input to provide the vital role of that functional group in our body. Hence, from the experimental evidences mentioned above, the fact is also verified in our model system that in the presence of carbon quantum dots with various functional groups, it is evident that the $-NH_2$ (amine) functionality on carbon quantum dots has significant interaction with PHOS VES, which is taken as the model system for the cell membrane. Very recently, scientists reported that nanoparticle binding to the bacterial membrane depends on the natural organic matter adsorbed onto them in the aqueous medium.[50] Such type of adhesion dictates the nanomaterial to behave differently to other surfaces. So, this also may be influenced by the functional group or other characteristics of the molecules, as observed in our study.

Conclusions

Functionalized carbon dots have been extensively used in drug delivery applications. However, it is of paramount important to know possible interaction between the functionalized carbon dots and cell membrane for effective use of such material in biomedical applications. In this work, an attempt has been made to address this issue. The interaction studies involving phosphatidylcholine vesicles (as the model cell membrane) and four different carbon dots bearing different functional groups ($-COOH$, $-NH_2$, $-OH$, and BSA coated) were conducted *in vitro* using various tools like PL behavior, surface charge on vesicles, QCM, ITC, and others. From the above studies, it was observed that the $-NH_2$ terminating carbon dots were capable of binding strongly with vesicles in comparison to other functional groups bearing carbon dots. This observation was also supported by direct visual evidence (TEM image), which shows that NH_2 functionalized carbon quantum dots (PEICD) have greater affinity towards PHOS VES. The mechanistic insight presented in the paper demonstrate higher H-bonding, signifying better interaction between the $-NH_2$ functionalized carbon dots and PHOS VES. Moreover, the transport of neurotransmitters (which are generally amine compound) in neurons for cellular communication through the synapse is only possible through vesicular platforms. This shows that in our body, such interactions are already present. In addition, the fact that the majority of the drugs have amine functionality also indicates that the probable $-NH_2$ functionality is favorable. Although the study was done *in vitro* to study the interaction of different functional carbon quantum dots and vesicles, such insight study of the nano–bio interface will open up a new horizon for biomedical

researchers for designing efficient carbon-based nanomaterials as drug/gene delivery vehicles.

Author contributions

J. S. B. and D. C. designed the experiment; J. S. B. performed the experiments; J. S. B., K. S. and D. C. analyzed the data; J. S. B., K. S. and D.C. wrote the manuscript.

Conflicts of interest

There are no conflicts to declare.

Acknowledgements

References

1 J. Douliez, V. Zhendre, A. Grelard and E. J. Dufourc, *Langmuir*, 2014, **30**, 14717–14724.

2 G. T. Kozma, T. Meszaros, I. Vashegyi, T. Fulop, E. Orfi, L. Dezsi, L. Rosivall, Y. Bavli, R. Urbanics, T. E. Mollnes, Y. Barenholz and J. Szebeni, *ACS Nano*, 2019, **13**(8), 9315–9324.

3 T. Huang, Z. Hou, Q. Xu, L. Huang, C. Li and Y. Zhou, *Langmuir*, 2017, **33**, 340–346.

4 G. Qing, N. Gong, X. Chen, J. Chen, H. Zhang, Y. Wang, R. Wang, S. Zhang, Z. Zhang, X. Zhao, Y. Luo and X. Liang, *Biophys. Rep.*, 2019, **5**, 184–198.

5 M. Gupta, U. Agrawal, V. Sharma and S. P. Vyas, *Liposomal Delivery Systems: Advances and Challenges*, ed. A. Samad, S. Beg, and I. Nazish, Future Science Ltd, London, 2015, vol. 1, ch. 6, pp. 75–86. DOI: DOI: 10.4155/fseb2013.14.30.

6 Z. Chen, Y. Tu, D. Zhang, C. Liu, Y. Zhou, X. Li, X. Wu and R. Liu, *Biomater. Sci.*, 2020, **8**, 4299–4307.

7 K. Hayashi, M. Watanabe, T. Iwasaki, M. Shudou and R. M. Uda, *Photochem. Photobiol. Sci.*, 2019, **18**, 1471–1478.

8 E. N. Towns, A. N. Parikh and D. P. Land, *J. Phys. Chem. C*, 2015, **119**(5), 2412–2418.

9 M. Hirai, S. Sato, R. Kimura, Y. Hagiwara, R. Kawai-Hirai, N. Ohta, N. Igarashi and N. Shimizu, *J. Phys. Chem. B*, 2015, **119**(8), 3398–3406.

10 A. J. Urquhart and A. Z. Eriksen, *Drug Discovery Today*, 2019, **24**(8), 1660–1668.

11 C. J. Genito, Z. Beck, T. W. Phares, F. Kalle, K. J. Limbach, M. E. Stefaniak, N. B. Patterson, E. S. Bergmann-Leitner, N. C. Waters, G. R. Matyas, C. R. Alving and S. Dutta, *Vaccine*, 2017, **35**, 3865–3874.

12 M. Gaillard, A. Thuaire, G. Nonglaton, V. Agache, Y. Roupioz and C. Raillon, *Analyst*, 2020, **145**, 1997–2013.

13 P. K. Gaur, S. Mishra and S. Purohit, *Artif. Cells, Nanomed., Biotechnol.*, 2016, **44**(7), 1684–1693.

14 F. Giulimondi, L. Digiacomo, D. Pozzi, S. Palchetti, E. Vulpis, A. L. Capriotti, R. Z. Chiozzi, A. Laganà, H. Amenitsch, L. Masuelli, M. Mahmoudi, I. Screpanti, A. Zingoni and G. Caracciolo, *Nat. Commun.*, 2019, **10**(1), 3686.

15 L. Ou, S. Liu, X. Chu, G. Shen and R. Yu, *Anal. Chem.*, 2009, **81**, 9664–9673.

16 N. Gogoi, M. Barooah, G. Majumdar and D. Chowdhury, *ACS Appl. Mater. Interfaces*, 2015, **7**, 3058–3067.

17 A. Konwar, U. Baruah, M. J. Deka, A. A. Hussain, S. R. Haque, A. R. Pal and D. Chowdhury, *ACS Sustainable Chem. Eng.*, 2017, **5**(12), 11645–11651.

18 L. Dykman and N. Khlebtsov, *Chem. Soc. Rev.*, 2012, **41**, 2256–2282.

19 A. Llevot and D. Astruc, *Chem. Soc. Rev.*, 2012, **41**, 242–257.

20 E. C. Dreaden, A. M. Alkilany, X. Huang, C. J. Murphy and M. A. El-Sayed, *Chem. Soc. Rev.*, 2012, **41**, 2740–2779.

21 L. Cheng, X. Jiang, J. Wang, C. Chen and R. Liu, *Nanoscale*, 2013, **5**, 3547–3569.

22 I. Lynch and K. A. Dawson, *Nano Today*, 2008, **3**, 40–47.

23 J. S. Boruah and D. Chowdhury, *ChemistrySelect*, 2019, **4**, 4347–4354.

24 J. S. Boruah and D. Chowdhury, *Appl. Nanosci.*, 2020, **10**, 2207–2218.

25 S. Behzadi, V. Serpooshan, W. Tao, M. A. Hamaly, M. Y. Alkawareek, E. C. Dreaden, D. Brown, A. M. Alkilany, O. C. Farokhzad and M. Mahmoudi, *Chem. Soc. Rev.*, 2017, **46**(14), 4218–4244.

26 Q. Mu, G. Su, L. Li, B. O. Gilbertson, L. H. Yu, Q. Zhang, Y. Sun and B. Yan, *ACS Appl. Mater. Interfaces*, 2012, **4**, 2259–2266.

27 Q. Mu, G. Jiang, L. Chen, H. Zhou, D. Fourches, A. Tropsha and B. Yan, *Chem. Rev.*, 2014, **114**(15), 7740–7781.

28 X. Chen, F. Tian, X. Zhang and W. Wang, *Soft Matter*, 2013, **9**, 7592–7600.

29 J. Yang, Y. Hu, R. Wang and D. Xie, *Soft Matter*, 2017, **13**, 7840–7847.

30 M. Laurencin, T. Georgelin, B. Malezieux, J. M. Siaugue and C. Menager, *Langmuir*, 2010, **26**(20), 16025–16030.

31 F. Mousseau, E. K. Oikonomou, V. Baldim, S. Mornet and J. Berret, *Colloids Interfaces*, 2018, **2**(4), 50.

32 Y. Liu, S. Li, X. Liu, H. Sun, T. Yue, X. Zhang, B. Yan and D. Cao, *ACS Appl. Mater. Interfaces*, 2019, **11**(27), 23822–23831.

33 N. Kanwa, M. Kavana and A. Chakraborty, *Langmuir*, 2020, **36**, 10628–10637.

34 S. Burgess, A. Vishnyakov, C. Tsovko and A. V. Neimark, *J. Phys. Chem. Lett.*, 2018, **9**, 4872–4877.

35 M. Murakami, H. Yoshikawa, K. Takada and S. Muranishi, *Pharm. Res.*, 1986, **3**, 35–40.

36 R. Ludmerczki, S. Mura, C. M. Carbonaro, I. M. Mandity, M. Carraro, N. Senes, S. Garroni, G. Granozzi, L. Calvillo, S. Marras, L. Malfatti and P. Innocenzi, *Chem.–Eur. J.*, 2019, **25**, 11963–11974.

37 B. Han, Y. Li, T. Peng, M. Yu, X. Hu and G. He, *Anal. Methods*, 2018, **10**, 2989–2993.

38 J. Gogoi and D. Chowdhury, *J. Mater. Sci.*, 2020, **55**, 11597–11608.

39 G. E. G. Jothi, S. Kamatchi and A. Dhathathreyan, *J. Chem. Sci.*, 2010, **122**(3), 341–348.

40 G. Sauerbrey, *Z. Phys.*, 1959, **155**, 206–222, DOI: 10.1007/BF01337937.

41 P. J. Huang, F. Wang and J. Liu, *Langmuir*, 2016, **32**(10), 2458–2463.

42 Y. Sudo, M. Yamabi, S. Kato, C. Hasegawa, M. Iwamoto, K. Shimono and N. Kamo, *J. Mol. Biol.*, 2006, **357**, 1274–1282.

43 H. Osanai, T. Ikehara, S. Miyauchi, K. Shimono, J. Tamogami, T. Nara and N. Kamo, *J. Biophys. Chem.*, 2013, **4**, 11–21.

44 O. Mertins and R. Dimova, *Langmuir*, 2011, **27**(9), 5506–5515.

45 B. Qu, L. Guo, X. Chu, D. Wu, G. Shen and R. Yu, *Anal. Chim. Acta*, 2010, **663**, 147–152.

46 E. A. Robinso, *Can. J. Chem.*, 1963, **41**, 173–179.

47 L. E. Eiden, *FASEB J.*, 2000, **14**(15), 2396–2400.

48 J. V. Liefferinge, A. Massie, J. Portelli, G. D. Giovanni and I. Smolders, *Front. Cell. Neurosci.*, 2013, **7**, 139, DOI: 10.3389/fncel.2013.00139.

49 R. D. Blakely and R. H. Edwards, *Cold Spring Harbor Perspect. Biol.*, 2012, **4**, a005595, DOI: 10.1101/cshperspect.a005595.

50 S. Li, S. Wang, B. Yan and T. Yue, *ACS Sustainable Chem. Eng.*, 2021, **9**(41), 13705–13716.